doi.org/10.1016/j.intermet.2021.107129

Creep behaviour of two-phase lamellar TiAl: Crystal plasticity modelling and analysis

M. Umer Ilyas*, M. Rizviul Kabir**
Institute of Materials Research
German Aerospace Center (DLR),
Linder Hoehe, 51147 Cologne, Germany

Abstract

Two-phase ($\alpha_2Ti_3Al+\gamma TiAl$) fully lamellar TiAl alloys show highly anisotropic creep behaviour. Depending on lamellar orientations, locally in the TiAl phases hard and easy deformation modes are active, which significantly influence the creep behaviour at a global scale. To obtain comprehensive understanding how the locally activated crystallographic deformation modes influence the macroscopic creep behaviour, a crystal plasticity (CP) model with modified hardening behaviour is proposed in this work. For this purpose, a softening parameter is introduced in the model that phenomenologically describes the threshold stresses for material softening depending on pile-up dislocation lengths during creep deformation. The model allows us to interpret the cause of creep anisotropy at macro-scale deformation based on the orientation dependent activation and interactions of slip systems at the TiAl phases. Comprehensive study was performed to validate the model and to predict creep parameters under different temperature and stress loading conditions. Comparing the experimental data with simulation results, we found that the proposed CP model captures creep behaviour in primary, secondary, and tertiary regime for all the lamellar orientations with good accuracy. This model can be further used for investigating microstructure-sensitive creep behaviour of a wide range of TiAl alloys.

Keywords:
Crystal Plasticity, Creep anisotropy, Lamellar TiAl alloy, Finite element modelling

* Corresponding author. umerilyas4@gmail.com
** Corresponding author. mohammad-rizviul.kabir@dlr.de, Tel.: +49 2203 6012481

1. Introduction

Multi-phase TiAl alloys are increasingly used in aero-engine turbine blades due to their low specific weight and good thermo-mechanical properties. New generation of TiAl alloys with improved creep resistance are of great interest for these high temperature applications [1]. Designing materials with excellent creep properties requires in-depth micromechanical understanding of the microstructure-property correlations. Today's advancement in computational methodologies allows us to investigate micromechanical fundamentals over different structural length scales using complex, physics based constitutive models. For TiAl alloys, available computational approaches to model creep behaviour of TiAl alloys are somewhat limited, although, room and high temperature deformation modelling considering scale bridging micromechanical interactions has been established in last few decades [2–7]. Present work focuses on the improvement of current modelling approaches to characterize creep behaviour of TiAl alloy considering two-phase ($\alpha_2Ti_3Al+\gamma TiAl$) lamellar microstructure.

In past few decades, experiments were conducted to identify key roles of microstructure on creep resistance of TiAl alloys. Systemic analyses were performed on bulk materials of single TiAl phases [8,9], combined ($\alpha_2Ti_3Al+\gamma TiAl$) multi-phases with lamellar structures, known as PST-TiAl [10–12], and polycrystals of single and multi-phase lamellar grains [12–14]. It was found that the creep responses of single TiAl phases and multi-phase combinations were significantly different, which comes from different inherent boundaries. For example, phase boundaries between α_2/γ, γ/γ lamellae for the case of lamellar structure, and for the case of polycrystals, additional grain boundaries among γ-grains and lamellar grains. Due to anisotropic phase properties and textured phase arrangements, the morphology plays an important role on the macroscopic creep responses.

In predictive analysis the computational methodologies should consider the most dominant microstructural features as well as the constitutive behaviour related to the lower scale deformation micromechanisms considering anisotropy and orientation information.

Early works of creep modelling frequently used empirical power-law formulations as follows [18-20]

$$\dot{\varepsilon}_{ss} = A \exp\left(-\frac{Q}{R\,T}\right)\sigma^n, \qquad (1)$$

where $\dot{\varepsilon}_{ss}$ is secondary stage creep rate, A is a structure factor, Q is the activation energy for creep, R is the gas constant, T is the temperature, σ is applied stress, and n denotes the stress exponent. For multi-phase TiAl alloys, modelling of creep was based on this empirical power-law so far [15]. Continuum creep-damage model was also proposed for analysing creep curves of TiAl alloys [16]. These computational approaches evaluated local stresses and strains during creep process in terms of effective quantities over phase domains, but the underlying causes of evolving stresses and strains as a resultant of crystallographic deformation interactions had not been focused.

To understand effective macroscopic deformation based on the lower scale interactions of crystallographic deformation processes in metallic and intermetallic phases, crystal plasticity (CP) viscoplastic models were adopted in many advanced computational approaches [17,18]. These models took similar power-law functions of **Eq. 1**, which acted over local material volumes or phases, and take into account the crystallographic slips as the main deformation mechanisms. Thus, CP models allow comprehensive understanding on how activation and interactions of slip systems contribute to the effective stress and strainformation under applied load and temperature. Recently, some authors extended the CP models for creep simulation in Ni-based [19–24] and Ti-based alloys [25,26]. However, no CP models were suggested for predicting TiAl creep behaviour so far. Such model is, however, required to explore lower scale salient features of multi-phase constituents of TiAl intermetallic phases which are important for understanding macroscopic creep behaviour and to establish microstructure-property correlations. Under this circumstance, in the present work we propose an extension of CP model to investigate the anisotropic nature of creep curves of TiAl-lamellar microstructure and to gain insights into the creep mechanisms. Thus, the main objectives are:

(1) Extending a previously developed temperature and rate sensitive CP model [7] for simulating creep behaviour of fully lamellar two-phase TiAl microstructure: This model uses a rate-enhanced power-law formulation to take into account the variation of strain rate sensitivity at different temperatures. In the current work, we propose a modified hardening behaviour, which incorporates a softening parameter for degrading material. The softening parameter has been empirically defined from the knowledge of microstructure degradation observed during creep experiments on lamellar PST-TiAl alloy.

(2) Model validation and predictive analysis of anisotropic creep behaviour of fully lamellar PST-TiAl: Detailed simulations are performed to study the sensitivity of the model against anisotropic creep of fully lamellar PST-TiAl alloy. Further, in-depth understanding of

the creep behaviour is provided by analysing steady state creep rate and creep activation parameters (such as activation volume and activation energies) of fully lamellar TiAl microstructure. Moreover, influence of the proposed softening parameter on the creep strain evolution has been studied to understand creep behaviour in secondary or tertiary creep regime under different temperature and stress conditions.

2. Creep behaviour of lamellar TiAl crystal

In past decades the fully lamellar PST-TiAl alloy, which consists of two TiAl phases, namely γTiAl and α_2Ti_3Al, has been investigated for the fundamental understanding of creep resistance in lamellar microstructure [10–12,27–29]. Parthasarathy et al. [12] investigated anisotropic creep behaviour of a PST-TiAl with nominal composition of Ti-48at.%Al. Creep experiments for different temperature ranges and stress regimes were performed for three basic lamellar orientations, θ=0°, 45°, and 90°. The results showed low creep resistance for 45° oriented lamellar arrangement and higher creep resistance for 0° and 90° orientations. Further, they correlated the creep activation energies of lamellar microstructures in terms of anisotropy and applied loading, e.g. temperature and stress regimes.

As known from PST deformation analysis [30–33], for 45° oriented lamellae crystallographic deformation occurs parallel to the lamellar interfaces, resulting in easy deformation of the lamellar grains. This lamellar arrangement is denoted as “soft deformation mode”, where the deformation occurs “longitudinal” with respect to the lamellar interfaces. For 0° and 90° orientations, crystallographic deformation occurs across lamellar thickness. Deformation occurs mostly “transverse” to the lamellar interface for 90° orientation and in a mixed form of “longitudinal” and “transverse” for 0° orientation. For both cases lamellae are hard to deform. These orientations of the lamellae are denoted as “hard deformation mode”. The crystallographic deformation modes observed in room temperature uniaxial tests are the same for the case of high temperature plastic deformation as well as for creep, but their activation energies vary to some degree depending on material’s chemical composition and lamellae arrangements.

Using a different lamellar PST-TiAl (nominal composition Ti-49.5at%Al) Wegmann et al. [11] conducted a similar set of creep experiments. The tests were conducted at 1150 K but for different stress regimes. They used 35° and 55° lamellar orientations as soft

deformation mode. For the hard deformation mode, 0° and 90° were tested. The experiments also showed anisotropic nature of creep behaviour in strain and strain rate evolution (**Fig. 1)**.

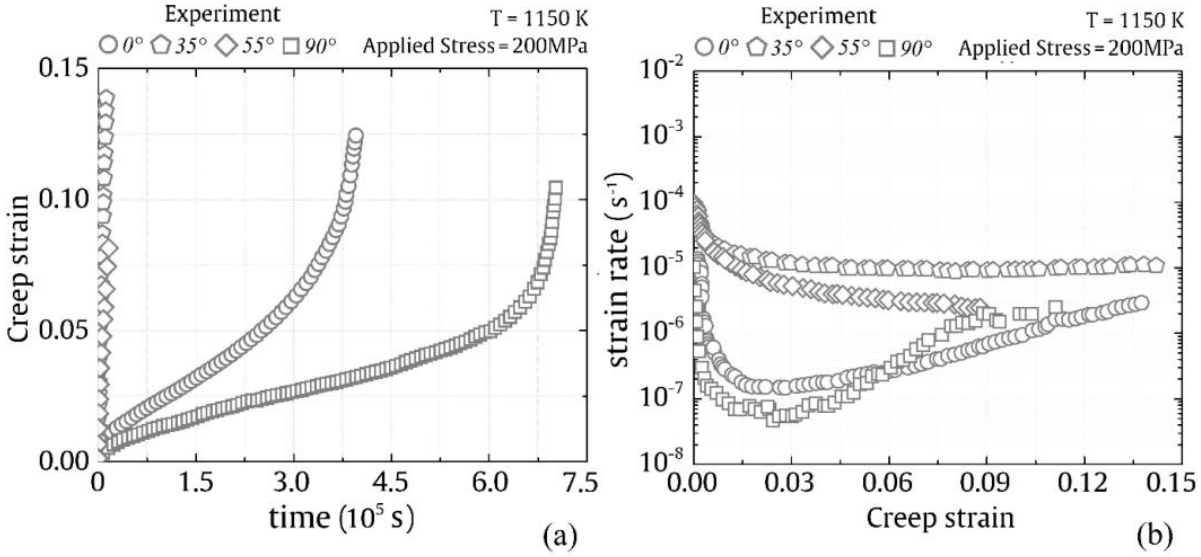

Figure 1*: Creep deformation of PST Ti-49.5at%Al crystals at different lamellar orientations. (a) Creep strain vs time, (b) Creep rate vs creep strain. Regenerated from Wegmann et al.* [11] *with permission.*

For all the lamellar PST-TiAl alloys, soft deformation modes result in higher creep strain rate and low creep resistance, and for hard deformation mode, lower creep rate and higher creep resistance. The anisotropy effect is distinguishable in primary, secondary, and tertiary creep regimes. For high temperature and high stress range, creep resistance of the lamellar microstructure decreases. Microstructural instability in terms of lamellar refinement was observed during high temperature creep. With an increased temperature coarsening in lamellar microstructure occurs, which influences the strain rate during creep [28].

Experimental observations of anisotropic creep phenomena have been explained in terms of morphology and active slip deformation modes, which evolves with respect to time, temperature, and stress regime. The increased number of lamellar interfaces plays an important role for increased creep resistance, and the spacing between the lamellae, which controls the dislocation density during creep deformation, inversely influences the creep resistance [34].

The activated mechanisms for crystallographic deformation depend mainly on the orientation of lamellar plates with respect to loading angle. In hard deformation mode, the creep resistance was observed to be higher as compared to soft deformation mode [11]. In hard deformation mode the required critical resolved shear stress (CRSS) to activate transversal slips is higher than that of longitudinal slips in soft deformation mode [32]. Also,

depending on the angle of lamellar interfaces with respect to the load direction, the motion of dislocations is hindered by boundaries, and this hindering is stronger in hard deformation mode as compared to the soft deformation mode. Lowest steady state creep rates were observed for hard deformation mode, which were approximately two orders of magnitude lower than for the soft deformation mode.

To understand creep micromechanisms based on the lower scale deformation of intermetallic phases, a strain rate enhanced crystal plasticity model was adopted. The model incorporates fundamental crystallographic deformation for γTiAl and α_2TiAl crystals, which are listed in **Table 1** in **Appendix A**. These slip systems were grouped according to the deformation modes of lamellar microstructure, namely, longitudinal, transversal, and mixed, which were active under uniaxial loading when lamellae are oriented 0°, 45°, and 90° with respect to the loading axis [31]. The deformation modes of the slip systems for 0° and 90° orientation were generalized as "hard" deformation modes, and for 45° they were named as "soft" deformation modes.

3. Numerical Approach

3.1 Rate enhanced Crystal plasticity

In a previous work [7], a strain rate enhanced CPFEM model was proposed for high temperature deformation behaviour of two-phase TiAl alloy. The model incorporated a physically motivated enhancement of strain-rate sensitivity (SRS) parameter in the power-law equation, allowing the simulation of anisotropic deformation behaviour of lamellar PST-TiAl alloy for a wide range of temperature.

The theoretical framework was adopted from a classical crystal plasticity model [17,18,35]. To calculate the shear strain rate of a slip system α, following rate dependent viscoplastic power law formulation was proposed

$$\dot{\gamma}^{\alpha}=\begin{cases} \dot{\gamma}_0 \left|\frac{\tau^{\alpha}}{g^{\alpha}}\right|^{\frac{1}{\tilde{m}}} \operatorname{sgn}(\tau^{\alpha}), & \text{if} \quad g_{\mu}^{\alpha}<\tau^{\alpha}< g^{\alpha} \\ 0, & \text{otherwise} \end{cases} \qquad (2)$$

where $\dot{\gamma}_0$ is initial shear strain rate, τ^{α} is the resolved shear stress, g^{α} is the mechanical threshold stress, and $\tilde{m}$ is the strain rate sensitivity (SRS) parameter of slip system α, and g_{μ}^{α} is athermal part of mechanical threshold stress.

The values of $\tilde{m}$ vary from 0 to 1 and characterize the response of material towards the change of strain rates. Rate sensitive material deformation will have $\tilde{m}$ closer to 1, whereas values closer to 0 mean rate independent plasticity.

This $\tilde{m}$ parameter takes the effect of dislocation glide and climb on strain rate sensitivity of the material into account. It was formulated as a function of strain rate and temperature as follows [7],

$$\tilde{m} = \frac{\left(\dot{\gamma}^{\alpha}+\dot{\beta}^{\alpha}\right)\frac{k_b T}{F_0}\frac{1}{pq}\left(\frac{R^{\alpha}k_b T}{F_0}\right)^{\frac{1}{q}-1}}{\dot{\gamma}^{\alpha}\left[1-\left(\frac{R^{\alpha}k_b T}{F_0}\right)^{\frac{1}{q}}\right]+\dot{\beta}^{\alpha}\left[\frac{k_b T}{F_0}\frac{1}{pq}\left(\frac{R^{\alpha}k_b T}{F_0}\right)^{\frac{1}{q}-1}\right]}, \qquad (3)$$

where, $\dot{\beta}^{\alpha}$ is strain rate of dislocation climb, T is the temperature, k_b is Boltzmann constant and F_0 is the activation energy needed to surpass the obstacle at 0 K. The parameters p and q are related to the shape of obstacle profile typically in range $0 \geq p \geq 1$ and $1 \geq q \geq 2$ [36]. The term $R^{\alpha} = \ln\left(\dot{\gamma}_i^{\alpha}/\dot{\gamma}^{\alpha}\right)$, where $\dot{\gamma}_i^{\alpha}$ is a constant of order 10^6 s^{-1} [37].

Using Orowan's law and assuming equilibrium concentration of vacancies, we took [7,37],

$$\dot{\beta}^{\alpha} = \frac{\rho_m b D_0 \Omega \sigma_n}{b k_b T}\exp\left(-\frac{\Delta Q_{sd}}{k_b T}\right) \qquad (4)$$

where ρ_m is mobile dislocation density, b is Burgers vector, D_0 is a material constant, Ω is atomic volume, ΔQ_{sd} is self-diffusion activation energy, and σ_n is resolved normal stress defined for each slip system α as $\sigma_n^{\alpha}=\sigma : n^{\alpha}\otimes n^{\alpha}$.

The mechanical threshold stress evolves by a hardening law as follows,

$$\dot{g}^{\alpha} = \sum_{\beta} h^{\alpha\beta}\left|\dot{\gamma}^{\beta}\right|, \qquad (5)$$

where, $h^{\alpha\beta}$ is instantaneous hardening modulus calculated as $h^{\alpha\beta} = q\, h^{\alpha\alpha}$, where q is a hardening matrix which describes self and latent hardening. For TiAl alloy, q values have not been determined experimentally, thus we assume q=1.0 for all slip systems, which implies that the effect of self and latent hardening is identical.

For HT deformation behaviour of lamellar PST-TiAl alloy, temperature sensitive Voce hardening law was used in [7]. This model predicts strain and stress evolution due to incremental loading quite satisfactory. However, this model lacks some assumptions of material softening at the high creep strain regime, which occurs due to the change or distortion of internal material structure. In this work, a modification in the hardening

behaviour has been proposed based on the work of Peirce et al. [17], where it is assumed that softening occurs after a saturation stress limit as follows

$$h^{\alpha}=h_0 \operatorname{sech}^2\left(\frac{h_0\gamma}{\tau_s-\tau_0}\right) - s^{\alpha}, \qquad (6)$$

where, h_0 is the initial hardening rate, τ_s is the saturation stress, τ_0 is the initial shear stress, γ is the cumulative strain on all slip systems, and s^{α} represents microstructural softening.

For the case of PST-TiAl, it has been observed that the acceleration of creep rate after reaching the steady state is attributed to microstructural softening due to coarsening of lamellae [28] in regions with high stress concentrations. These regions are lamellar boundaries whose spacing increase during creep deformation, whereas their density decreases indicating their dissolution [28]. Kishida et al. [33] made similar observations and attributed the softening in their stress strain curves to the relaxation of local stresses in the vicinity of lamellar boundaries. Based on these experimental observations, following empirical form of the softening parameter s^{α} is proposed to capture softening due to microstructural degradation of the two-phase lamellar structure,

$$s^{\alpha} = h_0 \ln\left(\frac{g^{\alpha}_{bd,0}}{g^{\alpha}_{bd}}\right), \qquad (7)$$

where, g^{α}_{bd} is part of mechanical threshold stress associated with resistance to plastic flow at microstructural boundaries, such as grain and lamellar boundaries, and $g^{\alpha}_{bd,0}$ is a reference threshold stress at 0 K. If the local stress concentration, g^{α}_{c} near lamellar boundary arises due to pileup of dislocations, the g^{α}_{bd} can be approximated as [7]

$$g^{\alpha}_{bd} = \left(\frac{2\mu b g^{\alpha}_{c}}{\pi\omega l_{pl}}\right)^{\frac{1}{2}}, \qquad (8)$$

where, l_{pl} is length of dislocation pileup at lamellar boundary, and $\omega=2(1-\vartheta)/(2-\vartheta)$ for an average dislocation character, with ϑ as Poisson's ratio. Stress concentration g^{α}_{c} should be temperature and strain rate dependent. At high temperatures, its values decrease implying a reduction in resistance to plastic flow at lamellar boundaries, thus increase in softening. At higher strain rates or high creep stresses, g^{α}_{c} should also vary, which may eventually influence the softening parameter s^{α}. In the present work, strain rate dependence of g^{α}_{c} is approximated in terms of shear modulus for each morphological group of slip system. Considering the limiting cases for **Eq.7**, very low g^{α}_{c} will lead to high s^{α}, whereas high g^{α}_{c} values will make s^{α} close to zero.

The influence of softening parameter, s^{α} on the creep curve is shown in **Fig. 2**. The magnitude of s^{α} serves as a controlling parameter for evolution of creep curve, particularly for the start of tertiary creep. High s^{α} values reduce creep time considerably and initiate tertiary creep stage earlier.

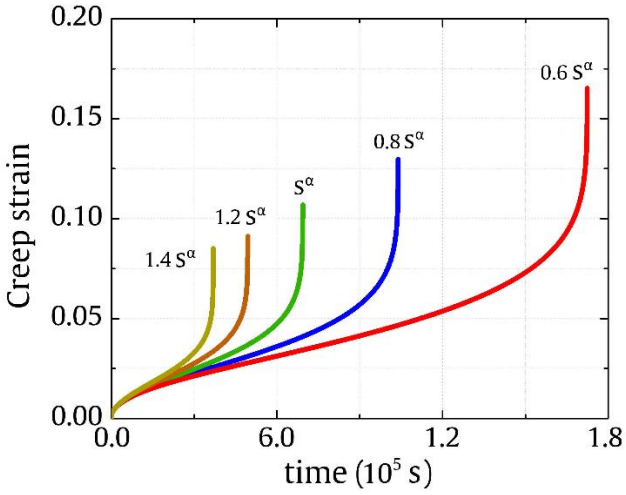

***Figure 2**: Influence of softening parameter s^{α} (assuming, s^{α}=140.0 MPa) on evolution of creep curves.*

3.2 FE modelling approach

Two-phase fully lamellar microstructure was modelled using a FE based Lamellar Unit Cell (LUC) to obtain stress-strain response of the PST-TiAl alloy. The LUC consisted of representative volume element (RVE) of γTiAl and α_2Ti3Al phases. Three RVEs were defined according to their present vol.% in a PST-TiAl alloy, one was for a γ-matrix lamellae, the others were for a γ-twin lamellae and a α_2-lamellae (**Fig. 3)**. According to [38], LUC with a minimum of 3 RVEs is sufficient to describe the most important micromechanical responses of lamellar PST-TiAl in numerical models.

The CP constitutive model was assigned to the LUC for describing deformation behaviour of the γTiAl and α_2Ti_3Al phases. Crystallographic orientation relationships between α_2 and γ-phases, and the anisotropic phase properties were described in the RVE elements.

Macroscopic effective stress and strain of the lamellar microstructure was calculated from the local stress-stain responses over the TiAl-phases described in the LUC with 3 RVEs. A two-scale micro-macro approach has been adopted for this purpose [5]. At micro-scale the RVEs deform according to the assigned CP constitutive behaviour of the TiAl phases,

whereas at macro-scale an average stress-strain response was obtained from the calculation of nodal deformation and reaction forces over the LUC boundaries. The LUC can be rotated arbitrarily at in a local coordinate system to obtain orientation dependent stress-strain response.

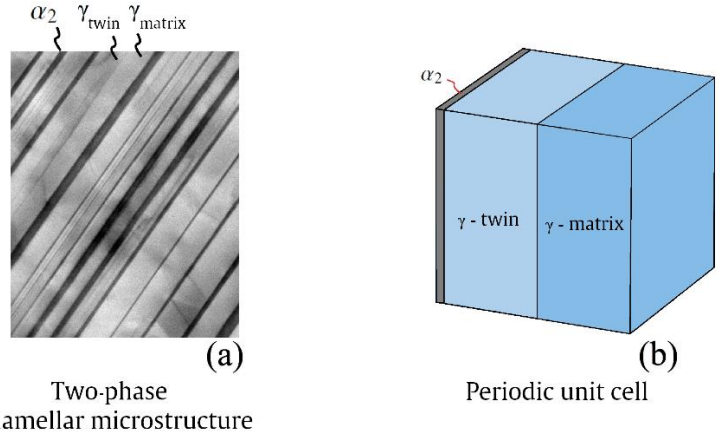

***Figure 3**: Lamellar microstructure, (a) two-phase lamellar microstructure with α_2-, γ-twin, and γ-matrix lamellar phases, (b) lamellar unit cell (LUC) model with idealized lamellar phases represented by RVEs*

CP model parameters were estimated for the known deformation modes of lamellar microstructure considering anisotropic deformation of PST-TiAl alloy [30,31]. Details of the parameter estimation using LUC for lamellar PST-TiAl and CP constitutive behaviour have been described elsewhere [38].

Taking (α_2+γ) lamellar configurations, ordinary, twin, and super slips of the γTiAl phase and prismatic, basal, and pyramidal slips of the α_2Ti_3Al phase were numerically estimated by adjusting the parameters of active slip systems that fit the experimental stress-strain response. To estimate all parameter sets, uniaxial experimental data corresponding to three lamellar orientations, θ = 0°, 45°, and 90° were required, which activate specific slip systems with respect to mixed, longitudinal, and transverse deformation modes of lamellar alloy. These parameter sets are listed in **Table 2** in **Appendix A**. Based on the experimental observation of Kishida et al. [31], the ordinary and twin slip strengths were assumed to be the same, but for the super slips some order higher values were taken, defined by fitting constants Q_{101} and Q_{112} [39].

4. Results and Discussion

4.1 Modelling anisotropic creep behaviour of PST-TiAl

In order to simulate the anisotropic creep deformation of lamellar PST-TiAl alloy, the CP parameters of the TiAl phases were re-evaluated. The starting parameter sets were taken from HT deformation of γTiAl phases [7]. Due to minor vol.% (ca 4 to 10%) and hard deformability of the α_2Ti$_3$Al phase, contribution of this phase to the overall creep deformation of lamellar alloy is minor. Hence, the α_2Ti$_3$Al parameters were kept fixed during the simulation. On the other hand, the major amount of ductile γTiAl phase contributes to the overall deformation, therefore, only the CP parameters of γTiAl phases were adjusted for PST-TiAl creep simulation.

The experimental data for creep deformation behaviour of PST Ti-49.5at%Al crystal were taken from the work of Wegmann et al. [10,11]. They performed a series of creep experiments considering several oriented lamellar configurations (θ=0°, 35°, 55°, 90°), where θ=0°, 90° results in hard and θ=35°, 55° results in soft deformation modes. The experiments were performed at 1150 K and with an applied stress of 200 MPa in compression. The complete set of model parameters was obtained by fitting the experimental hard and soft deformation modes by simulations. In soft deformation mode, model parameters were fitted for 45° lamellar orientation since the difference in creep behaviour of 35°, 45° and 55° orientation is minor. On the other hand, 0° and 90° creep curves were fitted for hard deformation modes for corresponding lamellar orientations. The CP parameters for the best fitted curves are listed in **Table 3** in **Appendix A**.

The experimental curves and the fitted simulations for anisotropic creep behaviour of PST-TiAl alloy are shown in **Fig 4**. The CP model with the proposed hardening-softening for.mulation satisfied the orientation dependent creep for soft and hard modes very well. Both the strain rate vs time (**Fig 4a**) and the strain rate vs creep strain (**Fig 4b**) curves matched with reasonable accuracy.

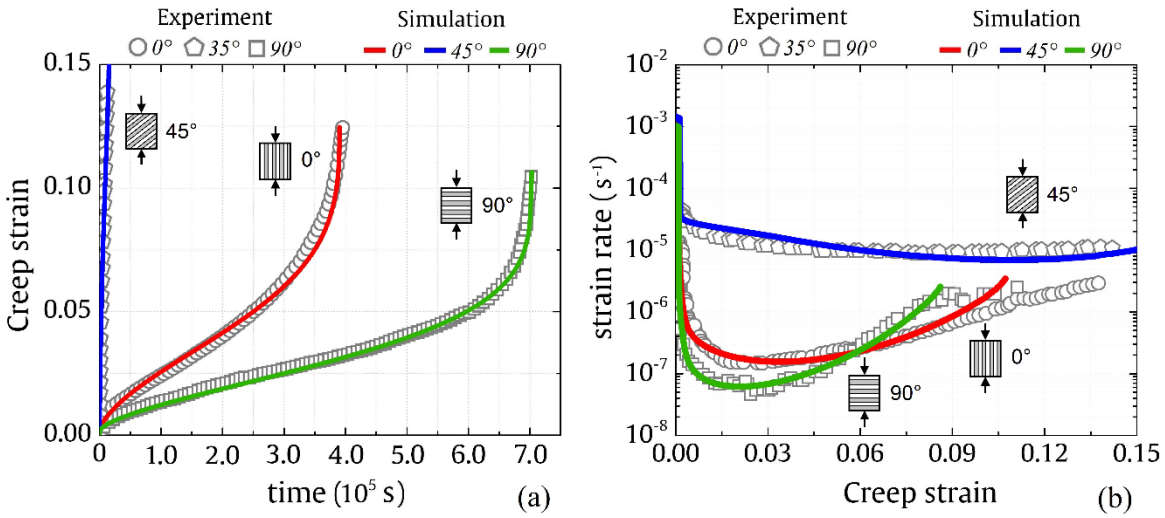

***Figure 4**: Creep simulation using best fitted CPFEM model parameters: (a) fitting of creep strain vs time, (b) fitting of strain rate vs creep strain. Experimental behaviour was obtained for PST Ti-49.5 at.%Al at different lamellar orientations, with an applied stress of 200MPa and temperature of 1150K from* [10,11].

In hard deformation mode, the lamellar boundaries of PST-TiAl are oriented perpendicular (90°) to the loading axis. This lamellar configuration exhibits higher creep resistance as compared to the orientation in which lamellar boundaries are parallel (0°) to the loading axis. Strain level at the beginning of creep (primary creep stage) is slightly higher for 0° as compared to 90° orientation, whereas creep time is longer for 90° orientation as compared to 0° orientation. Soft deformation mode exhibits lower creep resistance with shorter creep time and higher creep rate.

The observed differences in creep behaviour of PST-TiAl at different lamellar orientations can be associated with the role of lamellar boundaries which act as an effective barrier towards dislocation motion. In numerical simulation this effect was captured by the proposed g_{bd} parameter, which influences the softening s^{α} parameter. g_{bd} was adjusted to match the anisotropic softening at the tertiary regime.

During tertiary creep stage, the acceleration of creep rate or creep strain is more pronounced for 90° orientation as compared to other orientations. The difference in the tertiary creep stage of 0° and 90° orientations has been associated with deformation modes which are favourable for dynamic recrystallization [27]. However, in the presented model, this phenomenon has been captured phenomenologically by using higher values of parameter s^{α} for 90° orientation, which indicates the presence of higher amount of degraded material.

The proposed hardening model based on microstructural softening is able to predict creep deformation beyond secondary creep regime very well. To our knowledge, no CP

model was found that captures complete creep curves of fully lamellar PST-TiAl alloys considering anisotropic creep response.

4.2 Predictive analysis of creep deformation in α_2 and γ phases

The simulations provided additional knowledge of deformation behaviour on the length scale of the single phase microstructural features during creep. In **Fig. 5** local creep deformation curves were plotted based on individual phase wise deformation of γTiAl (matrix and twin) and α_2Ti_3Al. Data were evaluated for creep simulations of PST-TiAl crystal at T=1150 K and for applied stress of 200 MPa from the previous analysis (**Fig. 4**). **Fig. 5** shows creep strain vs time and strain rate vs creep strain for different lamellar orientations. As known from experiments, α_2Ti_3Al phase is highly creep resistant and its contribution to the overall deformation is very small[40]. A similar trend was observed in our calculations, which can be seen in **Fig. 5a,b,c,** indicating that the contribution of α_2Ti_3Al in creep deformation is the lowest for all lamellar orientations. Creep strains were highest in γTiAl phase, which significantly contributed to the overall deformation of lamellar microstructure.

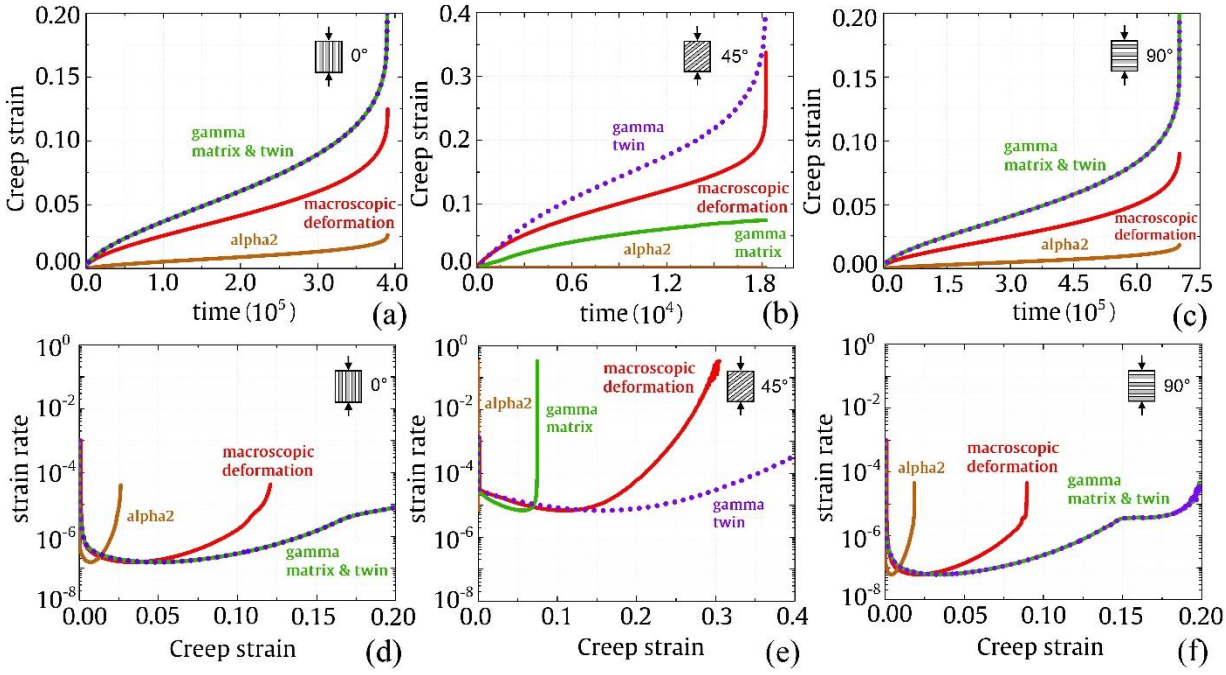

***Figure 5**: Simulation results for creep deformation of γ-matrix, γ-twin and α_2 phases with respect to macroscopic deformation in PST TiAl alloy at 1150K and with an applied stress of 200MPa. (a), (b), (c) show creep strain vs time responses for 0°, 45° and 90° lamellar orientation, and (d), (e), (f) show creep strain rate vs creep strain responses 0°, 45° and 90° lamellar orientation.*

The γ-matrix and γ-twin phases showed identical deformation trends for hard mode of deformation (**Fig 5a,c**) whereas for soft mode (**Fig 5b**), γ-twin deformation was higher compared to γ-matrix deformation. This behaviour was associated with the lower strain rate sensitivity of soft mode of deformation, where γ-twin lamellae deforms higher than γ-matrix lamellae, in contrast to the hard mode of deformation, where both γ-matrix and γ-twin lamellae show identical deformation trends [7]. Macroscopic creep deformation showed an average response from these phases. Due to less deformability of α_2Ti_3Al phase, it may not influence significantly the tertiary creep behaviour. As understood from the simulated creep strain rate behaviour (**Fig 5d,e,f**), mostly the ductile γ-phases (matrix and twin) contribute to macroscopic creep deformation in secondary and tertiary regime , rather than the brittle α_2Ti_3Al phase.

4.3 Analysis of creep stress exponents

Stress exponent, n_{ss} is an empirical constant associated with steady state creep rate (secondary creep regime). It was determined from log-log plot of applied stress and steady state creep rate, as

$$n_{ss}=\frac{\partial \log \dot{\varepsilon}_{ss}}{\partial \log \sigma} \qquad (9)$$

For PST-TiAl alloys, the experimentally determined stress exponent was about 7.5 for hard deformation modes with lamellar orientation parallel (0°) or perpendicular (90°) to the loading axis whereas for soft deformation mode, stress exponents were about 9.1 for 35° and 55° lamellar orientations [10,11,27].

For a similar PST-TiAl with slightly lower Aluminum content, Parthasarathy et al. [12] obtained stress exponents close to 5.0 for hard deformation mode. For soft deformation mode with 45° lamellar orientation, they evaluated stress exponents in the range of 4 to 5.

From creep simulations stated in previous section, the stress exponents were calculated using **Eq. 9** for hard and soft orientation modes. They were compared with the experimental results from Wegmann et al. [11] at T=1150 K. In **Fig 6(a)** the results are shown in a steady state creep strain ($\dot{\varepsilon}_{ss}$) vs. applied stress (σ) plot. For the hard orientation modes (θ = 0° and 90°) the stress exponent n_{ss} from the simulations matches very well with the experimental data. For the soft orientation, the simulated n_{ss} data was related to 45° orientation, which fell within the range of the experimental n_{ss} for 35° soft orientation.

Additional simulations were performed with new estimated CP parameters (**Table 3** in **Appendix A)** to predict the experimental n_{ss} for a different PST-TiAl as described by Parthasarathy et al [12]. In **Fig 6(b)** and **6(c)** the predicted n_{ss} from the simulations of different oriented lamellae (θ = 0°, 45°, 90°) and for two temperature range (T=1088 K, 1033 K) showed similar trend compared to the experimental behaviour.

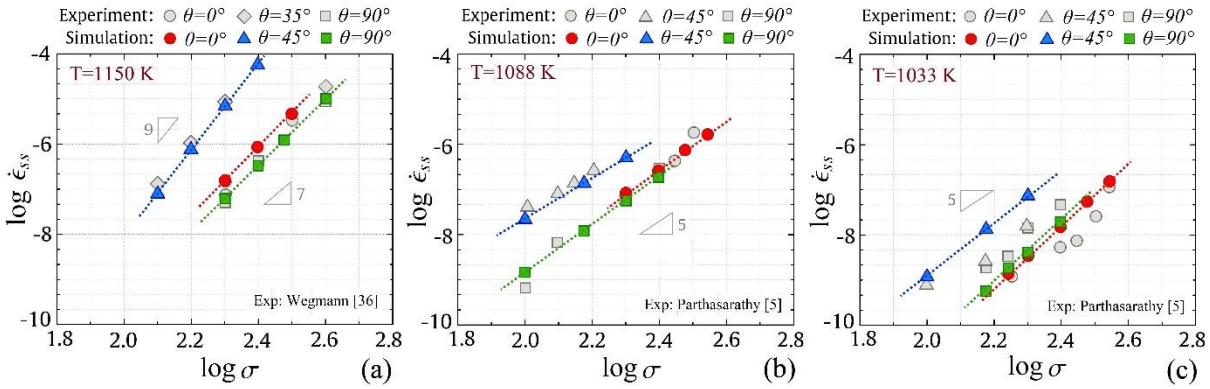

***Figure 6**: Model calculations of steady state creep rate ($\dot{\varepsilon}_{ss}$) with respect to applied stress (σ) for PST Ti-48% Al at different temperatures, (a) 1150K, experimental data is from* [10,11] *(b) 1088K and (c) 1033K, experimental data is from* [12]*. The slopes indicate the values of creep stress exponents.s*

Hard deformation mode has lower creep rates as compared to the soft deformation modes. This was mainly due to the orientation of lamellar boundaries with respect to the loading axis, which acted as an effective barrier in dislocation motion.

Comparing the strain rate data from **Fig 6**, we observe that the creep resistance decreases for both the hard and soft orientations if the applied temperature is higher, i.e., for 1150 K (**Fig 6a**) the creep strain rate is higher than for temperatures 1088 K and 1033K (**Fig 6b,c**). The increase of creep resistance with decreasing temperature can be associated with finer lamellar thickness at low temperatures. As the temperature increases, lamellar thickness increases resulting in reduction of creep resistance [28]. In simulations, this increase in creep resistance has been incorporated in the model by using a higher g_c value (which influences the softening parameter) representing high stress concentrations at lamellar boundaries, (see Section 3.1).

4.4 Dependency of creep behaviour on applied stress

Creep behaviour under different applied stresses was investigated and compared with the experimental observation. Kim et al [27,28] reported applied stress dependency of creep

behaviour for two “hard” lamellar orientations, θ = 0° and 90°. Commonly, with increasing applied stresses, creep occurs faster and the creep strain rate becomes higher.

For the same lamellar arrangements and applied stresses as reported in [27,28] simulations were performed. The best fitted simulations accord with the experimental curves very well, as shown in **Fig. 7**. **Fig 7a** and **7c** show that the simulated creep strain evolution with time coincides with the experiments for both orientations and for different applied stresses.

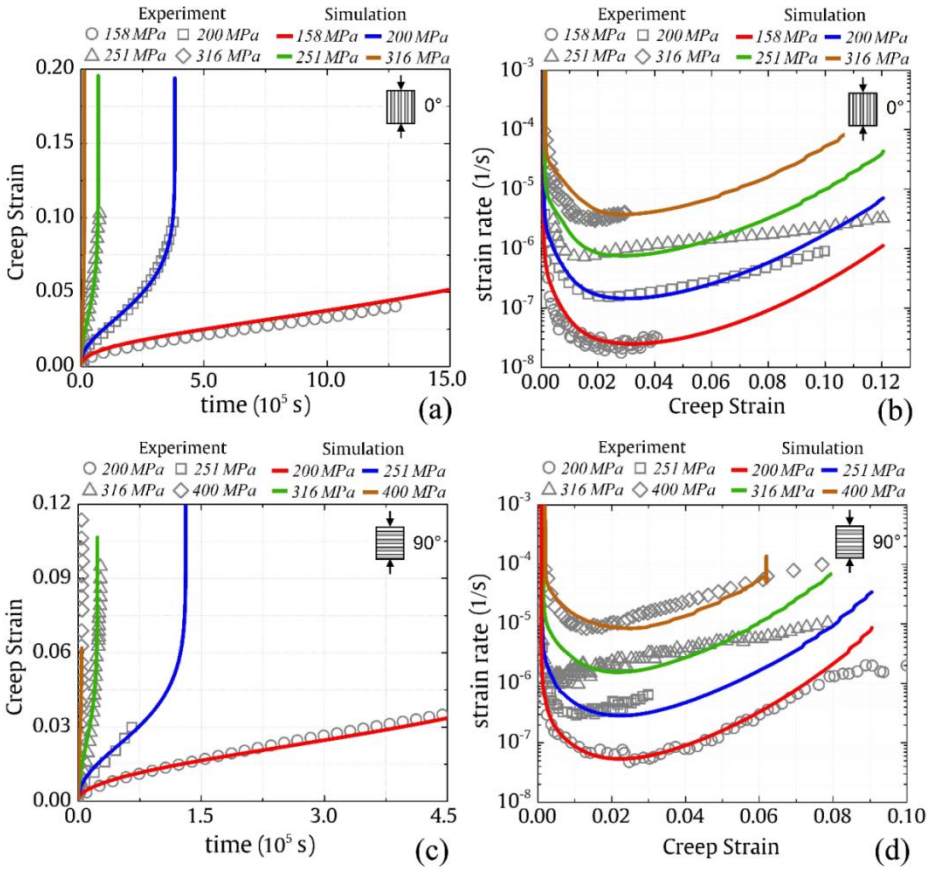

Figure 7: *Creep curves in hard deformation mode at different applied stress at 1150 K. (a) and (b) show creep strain vs time, (b) and (d) shos strain rate vs creep strain. Experimental data was taken from* [28] *for 0° orientation and* [27] *for 90° orientation.*

Simulated evolution of creep strain rate (**Fig 7b** and **7d**) also matches very well with experimental data. At the higher creep strain regime, the simulations predicted faster strain rate increase, whereas in the experiments the strain rate increased slowly and steadily. The proposed microstructure softening parameter s^{α} (compare equation 6) could be fitted to capture the experimental hardening-softening behaviour quite accurately.

4.5 Analysis of creep activation energy

Creep activation energy can be determined from Arrhenius plot of steady state creep rate and temperature. By incremental change in temperature, activation energy can be calculated using following relation,

$$Q_c = k_b T^2 \frac{\partial \ln \dot{\varepsilon}_{ss}}{\partial \ln T} \qquad (10)$$

Parthasarathy et al. [12] determined activation energies for creep of PST-TiAl crystals at 0°, 45°, and 90° lamellar orientations. Activation energies were orientation dependent. Highest values of 532±38 kJ/mol were measured when the lamellar boundaries were parallel (0°) to the loading axis. For 90° orientation, activation energies were 432±101 kJ/mol. In soft deformation mode, activation energies were 398 kJ/mol for 45° lamellar orientation.

Numerically the activation energies for oriented lamellae were calculated from the creep simulations using **Eq. 10** and fitted model parameters used for Parthasarathy et al. [12] specimens at 1088 K and 1033 K (**Fig. 6b,c**). Results are shown in **Fig. 8** for hard and soft mode orientations. The predictions are well within the range of activation energies reported by [12] for PST-TiAl crystals.

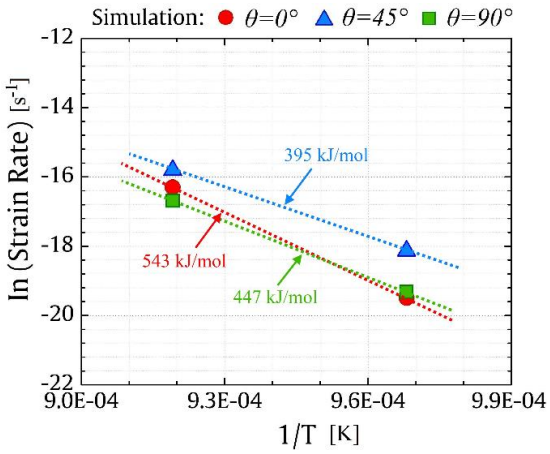

***Figure 8**: Activation energy calculations for PST-TiAl crystals from simulation results. Applied stress is 200MPa for hard deformation (0°,90°) and 150MPa for soft deformation (45°) mode.*

Compared to the self-diffusion activation energy of Ti (250 kJ/mol) and Al (358 kJ/mol) in γTiAl [41], the reported values of activation energies in PST-TiAl are higher. This means that, at these temperature ranges, diffusion is not an active mechanism in PST-TiAl crystals under creep conditions. For diffusion mechanisms to become active, the activation

energies must be equal to or near the self-diffusion activation energies of either Ti or Al. At high temperature creep the shear transfer through lamellar boundaries might play major role for these higher activation energies [12].

4.6 Analysis of strain rate sensitivity (SRS) during creep

Analysing the evolution of SRS parameter, $\tilde{m}$, an insight into the evolving strain rate during creep deformation under different applied stress and temperature was obtained. In **Fig. 9** the relationship among the creep strain, creep strain rate, and local evolution of $\tilde{m}$ was plotted for hard (θ=0° and 90°) and soft (θ=45°) lamellar orientations. Data were evaluated for creep simulations at 1150 K and for applied stresses of 200 and 300 MPa.

At the beginning of creep strain (i.e., primary creep regime) the strain rate and the SRS parameter $\tilde{m}$ decrease (point *a*). This trend was maintained until the minimum strain rates were achieved (point *b*). At this point, strain rate values are equal to the steady state creep rate in the secondary creep regime.

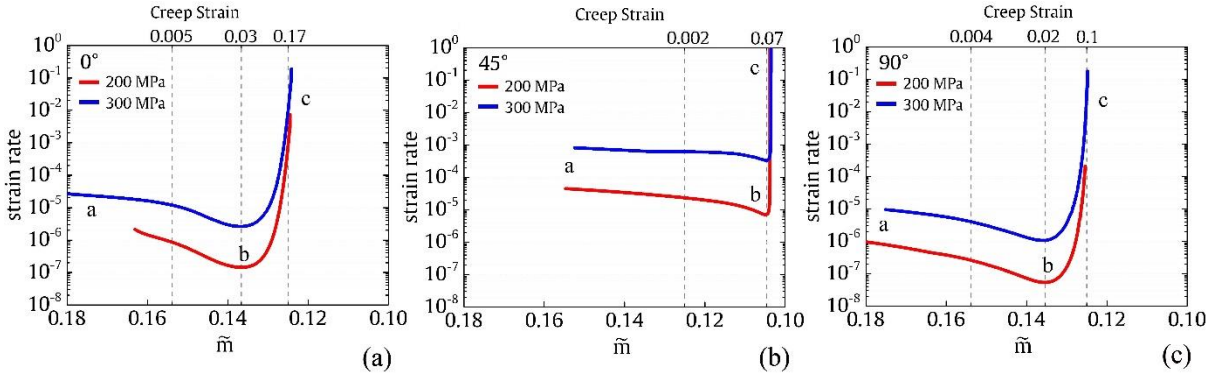

***Figure 9**: Variation of strain rate sensitivity parameter $\tilde{m}$ in creep simulation of a PST-TiAl crystal during creep deformation at 1150K.*

After point *b*, which is the beginning of tertiary creep regime, strain rate increases rapidly with slightly decreased $\tilde{m}$. In this regime, damage occurs drastically up to final failure (point *c*), and the resultant strain rate also increases drastically. Simulations predict only minor change in $\tilde{m}$ in tertiary creep regime.

This characteristic behaviour is almost the same for all lamellar orientations, see **Fig. 9a,b,c**. Only slight differences were found in the trend of decreasing strain rate with decreasing $\tilde{m}$ for soft (θ=45°) and hard (θ=0° and 90°) lamellar orientation. The transition of strain rate dependency as observed from *a* to *b* and then, from *b* to *c*, was smooth for orientations with hard mode deformation (**Fig. 9a,c**) as compared to the soft mode (**Fig. 9b**).

The creep strain evolution and m̃ analysis showed that the "steady state" at secondary creep (point *b*) and final tertiary creep (point *c*) was achieved at higher m̃ for 0° and 90° lamellar orientations (m̃=0.135 for *b*, and m̃=0.125 for *c*) compared to 45° orientation (m̃=0.105 for *b* and *c*). Lower m̃ values implying lesser strain rate sensitivity have been observed for soft deformation mode at room temperature [42] and at high temperatures [7]. This phenomena observed in the numerical simulation was due to the effect of the physically motivated rate-enhanced m̃ parameter (Eq. 3), which evolved depending on strain rate and temperature, in contrast to the constant strain rate sensitivity parameter in the classical CPFEM model that is insensitive to strain rate evolution.

Fig. 9 also summarizes the behaviour of m̃ and strain rate for two different stress levels (200 and 300 MPa). For both applied stresses, the curve trends for hard and soft lamellar orientations were similar, for higher applied stress only a higher strain rate occurred over the evolving creep strain and m̃.

4.7 Analysis of activation volumes

Activation volumes for creep deformation at different applied stress levels were calculated to understand dislocation mobility during high temperature creep in lamellar microstructure. The activation volume changes with average spacing and size of the obstacles. Thus, it can be correlated with the obstacle resistance that a moving dislocation needs to overcome along slip planes. The activation volume can be determined by using the following relation [43],

$$\Delta V = \frac{M_t k_b T}{\partial \sigma / \partial \ln \dot{\epsilon}} \qquad (11)$$

Here, M_t is the Taylor factor, which is defined as $M_t = \sum d\gamma / d\epsilon$, where $d\gamma$ is cumulative shear strain and $d\epsilon$ is macroscopic strain evaluated at the beginning of steady state creep. [54].

For PST-TiAl, M_t values were numerically estimated for three orientations, 0°, 45°, and 90°, using the proposed CP model. The simulation-based predictions of Taylor factors are in the similar range as those obtained by Dimiduk et al. [44], who calculated Taylor factors using analytical models for hard and soft mode orientations. Their determined M_t values were in the range of 2.0 – 3.0 for soft mode orientation, 2.5 for 0° orientation and 3.7

for 90° orientation. The calculated Taylor factors at T=1150 K are listed in **Table 4** in **Appendix A**.

The term, $\partial\sigma/\partial\ln\dot{\epsilon}$ in **Eq. 11** can be measured via stress jump in creep experiments at constant temperature. For the present case, we have performed numerical jump tests of the lamellar unit cell (LUC) model for three orientations, θ=0°, 45° and 90°.

The calculated activation volumes at steady state creep were potted against the applied stress for three temperatures, i.e. 1150 K, 1088 K and 1033 K (see **Fig. 10)**. For each orientation and temperature step, creep calculations were performed with a defined pre-stress and holding time, as applied in the experiments described in [12]. The results were depicted in solid points along with the experimental data in open points.

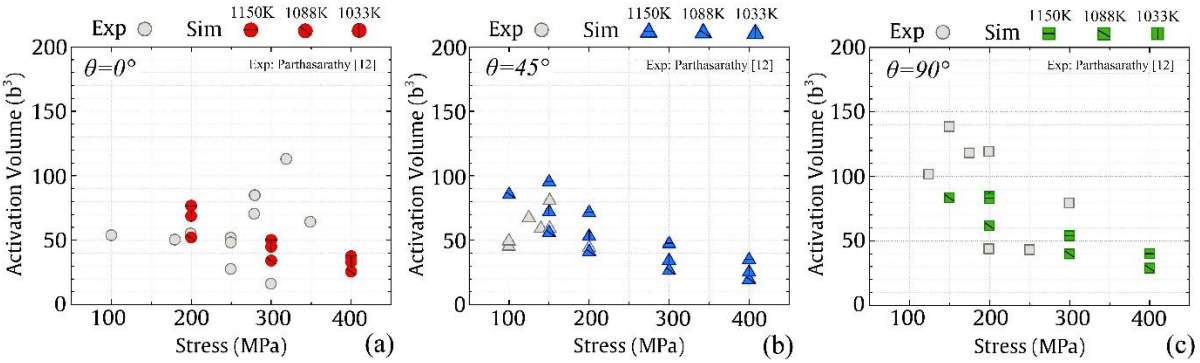

***Figure 10**: Activation volumes of PST-TiAl alloys at different lamellar orientations and stresses for different temperature increments. Experimental data is from* [12].

The simulations predicted a trend of decreasing activation volumes with the increase in creep stress, similar as the experimental observation. A similar trend of decreasing activation volumes with increasing stress has been observed in single phase γTiAl [45] and TiAl polycrystals [46]. Activation volumes are directly proportional to average length dislocations between obstacles [43]. As applied stress increases, the spacing between the obstacles decreases, which results in smaller activation volumes. In [47] the reduction in activation volume for higher stress had been associated with the decrease in obstacles spacing which reduces the swept area of dislocations to move past these obstacles. Numerical simulations show identical trend as observed in experiments, since high stress increases the creep rates until rupture as a result of reduced activation volume that aid the dislocation movement.

5. Conclusion

In this work we have proposed a modified hardening behaviour in an extension to a previously developed rate enhanced crystal plasticity (CP) model in order to capture anisotropic creep behaviour of fully lamellar two-phase TiAl alloy. The hardening model incorporates a softening parameter based on phenomenological observations of material degradation of lamellar microstructure.

This model has been verified for anisotropic creep deformation behaviour of PST-TiAl alloy for three lamellar orientation conditions, $\theta=0°$ (loading parallel to lamellar plate), causing a hard deformation mode, $\theta=45°$ (loading is 45° inclined to lamellar plate), causing a soft deformation mode, and $\theta=90°$ (loading perpendicular to lamellar plate), also causing a hard deformation mode. Detailed analyses with experimental validation show that the anisotropic creep behaviour for different temperatures and applied stress levels can be predicted with reasonable accuracy using this proposed model.

We also investigated creep parameters for lamellar TiAl alloy using CP based predictive analysis. For different stress and temperature levels our predictions showed similar creep stress exponents for soft and hard deformation modes, as they were found in the experiments. The model also predicted activation energies for anisotropic creep with a good match to the experimentally obtained data. Further, insights into the local creep of the TiAl single phases (α_2Ti_3Al and γTiAl) were obtained where we found that the γTiAl phases were the major contributor to the macroscopic creep deformation.

We found that in many aspects the presented CP model with physics-based improvements captures creep behaviour in primary, secondary, and tertiary regime for all lamellar orientations successfully. Most importantly, the proposed softening parameter, s^{α}, related to microstructure degradation, has served as essential controlling parameter of the creep curve evolution, particularly, at the tertiary creep regime. To our knowledge, the presented CP based modelling approach for TiAl alloy is the first one to capture the complete creep behaviour considering two-phase lamellar microstructure.

Based on well predicted results we found the proposed CP model is fully capable of describing creep behaviour of two-phase lamellar microstructure. To our view, the proposed CP model can be adopted as a useful tool for investigating microstructure-sensitive creep behaviour of a wide range of TiAl alloys.

Acknowledgements:

The authors gratefully acknowledge the financial support by the German Federal Ministry for Economic affairs and Energy under grant number 20E1504A. The authors thank Prof. Marion Bartsch for useful suggestions.

Appendix

Phase	Deformation modes			
	Longitudinal 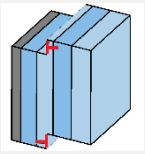	Mixed 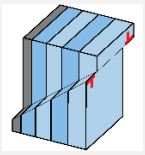	Transverse 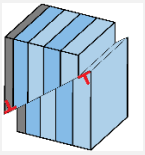	
γ-TiAl	(111)[1$\bar{1}$0] ordinary (111) [01$\bar{1}$] super (111) [10$\bar{1}$] super (111) [11$\bar{2}$] super (111) [11$\bar{2}$] twinning	(11$\bar{1}$)[1$\bar{1}$0] ordinary (1$\bar{1}$1) [10$\bar{1}$] super ($\bar{1}$11) [01$\bar{1}$] super	($1\bar{1}$1) [110] ordinary ($\bar{1}$11) [110] ordinary (11$\bar{1}$) [$\bar{1}$0$\bar{1}$] super ($\bar{1}$11) [$\bar{1}$0$\bar{1}$] super ($\bar{1}$11) [0$\bar{1}\bar{1}$] super ($1\bar{1}$1) [0$\bar{1}\bar{1}$] super	($\bar{1}\bar{1}$1) [$\bar{1}\bar{1}2$] super ($1\bar{1}$1) [$1\bar{1}2$] super ($\bar{1}$11) [$\bar{1}$12] super ($\bar{1}\bar{1}$1) [$\bar{1}\bar{1}2$] twinning ($1\bar{1}$1) [$1\bar{1}2$] twinning ($\bar{1}$11) [$\bar{1}$12] twinning
α_2-Ti_3Al	⟨11$\bar{2}$0⟩{0001} basal	⟨11$\bar{2}$0⟩{1$\bar{1}$00} prismatic	⟨$\bar{1}\bar{1}$26⟩{11$\bar{2}$1} pyramidal	

***Table 1**: Slip systems of TiAl based on morphological classification.*

Deformation Modes	**Slip**			
	Ordinary	Super 101	Super 112	Twin
Longitudinal	g_0^{long}	$g_0^{long}Q_{101}$	$g_0^{long}Q_{112}$	g_0^{long}
Mixed	g_0^{mix}	$g_0^{mix}Q_{101}$	$g_0^{mix}Q_{112}$	g_0^{mix}
Transverse	g_0^{trans}	$g_0^{trans}Q_{101}$	$g_0^{trans}Q_{112}$	g_0^{trans}

***Table 2:** Initial values of mechanical threshold stress g_0 at different deformation modes. Q_{101} and Q_{112} are additional strength factors associated with super dislocations according to* [39].

	Deformation modes					
	Wegmann'2000			Parathasarathy'2000		
Parameters	**Longitudinal**	**Mixed**	**Transverse**	**Longitudinal**	**Mixed**	**Transverse**
g_0 (MPa)	105.0	125.0	175.0	105.0	125.0	175.0
Q_{101}	1.5	1.5	1.5	1.5	1.5	1.5
Q_{112}	1.1	1.1	1.1	1.1	1.1	1.1
h_0 (MPa)	150.0	320.0	450.0	750.0	875.0	985.0
τ_s (MPa)	139.5	157.1	179.7	139.5	125.1	179.7
$\dot{\gamma}_0$ (s^{-1})	1.0e-4	2.5e-5	9.0e-4	7.0e-6	6.0e-5	5.0e-5
A (-)	0.485	0.436	0.436	0.32	0.35	0.35
g_c (MPa)	$0.0007\mu^a$, $0.0007\mu^b$	$0.0058\mu^a$, $0.0058\mu^b$	$0.0016\mu^a$, $0.0016\mu^b$	$0.0019\mu^a$, $0.0019\mu^b$	$0.0054\mu^a$, $0.0054\mu^b$	$0.0037\mu^a$, $0.0073\mu^b$
b (mm)	2.83e-7	2.83e-7	2.83e-7	2.83e-7	2.83e-7	2.83e-7
l_{pl} (mm)	0.001	0.001	0.001	0.001	0.001	0.001
g_{bd0} (MPa)	45	75	105	45	75	105

Table 3: *Set of model parameters for PST-TiAl alloy used for modelling specimens of Wegmann* [10,11] *and Parthasarathy* [12]. μ *is the shear modulus. Superscript* ^{a} *and* ^{b} *denote values used for 1033K and 1088K respectively.*

Stress (MPa)	**Taylor factors**		
	0°	**45°**	**90°**
125	--	2.36	--
200	3.28	2.36	3.65
300	3.22	2.34	3.52
400	3.21	2.30	3.46
Dimiduk [44]	2.5	2.0 - 3.0	3.7

Table 4: *Taylor factors at steady state creep stage estimated from proposed CPFEM model. Experimental taylor factors are taken from the work of Dimiduk* [44].

References

[1] B.P. Bewlay, S. Nag, A. Suzuki, M.J. Weimer, TiAl alloys in commercial aircraft engines, Mater. High Temp. 33 (2016) 549–559. https://doi.org/10.1080/09603409.2016.1183068.

[2] B.J. Lee, S. Ahzi, B.K. Kad, R.J. Asaro, On the deformation mechanisms in lamellar TiAl alloys, Scr. Metall. Mater. 29 (1993) 823–828. https://doi.org/10.1016/0956-716X(93)90234-J.

[3] E. Parteder, T. Siegmund, F.D. Fischer, S. Schlögl, Numerical simulation of the plastic behavior of polysynthetically twinned TiAl crystals, Mater. Sci. Eng. A. 192–193 (1995) 149–154. https://doi.org/10.1016/0921-5093(94)03229-7.

[4] R. Lebensohn, H. Uhlenhut, C. Hartig, H. Mecking, Plastic flow of γ-TiAl-Based polysynthetically twinned crystals: Micromechanical modeling and experimental validation, Acta Mater. 46 (1998) 4701–4709. https://doi.org/10.1016/S1359-6454(98)00132-3.

[5] M. Werwer, A. Cornec, Numerical simulation of plastic deformation and fracture in polysynthetically twinned (PST) crystals of TiAl, Comput. Mater. Sci. 19 (2000) 97–107. https://doi.org/10.1016/s0927-0256(00)00144-0.

[6] J.E. Butzke, S. Bargmann, Thermomechanical modelling of polysynthetically twinned TiAl crystals, Philos. Mag. 95 (2015) 2607–2626. https://doi.org/10.1080/14786435.2015.1070968.

[7] M. Umer Ilyas, M. Rizviul Kabir, Modelling high temperature deformation of lamellar TiAl crystal using strain-rate enhanced crystal plasticity, Mater. Sci. Eng. A. (2020) 139524. https://doi.org/10.1016/j.msea.2020.139524.

[8] K. Maruyama, T. Takahashi, H. Oikawa, Different origins of grain size and composition effects on creep in TiAl, Mater. Sci. Eng. A. (1992). https://doi.org/10.1016/b978-1-85166-822-9.50070-4.

[9] Y. Ishikawa, H. Oikawa, Structure change of TiAl during creep in the intermediate stress range, Mater. Trans. JIM. 35 (1994) 336–345. https://doi.org/10.2320/matertrans1989.35.336.

[10] G. Wegmann, T. Suda, K. Maruyama, Creep deformation of polysynthetically twinned (PST) Ti-48mol%Al, in: Key Eng. Mater., Trans Tech Publications, 2000: pp. 709–716. https://doi.org/10.4028/www.scientific.net/kem.171-174.709.

[11] G. Wegmann, T. Suda, K. Maruyama, Deformation characteristics of polysynthetically twinned (PST) crystals during creep at 1150 K, Intermetallics. 8 (2000) 165–177. https://doi.org/10.1016/S0966-9795(99)00081-3.

[12] T.A. Parthasarathy, P.R. Subramanian, M.G. Mendiratta, D.M. Dimiduk, Phenomenological observations of lamellar orientation effects on the creep behavior of Ti-48at.%Al PST crystals, Acta Mater. 48 (2000) 541–551. https://doi.org/10.1016/S1359-6454(99)00347-X.

[13] S. Bystrzanowski, A. Bartels, H. Clemens, R. Gerling, F.P. Schimansky, G. Dehm, H. Kestler, Creep behaviour and related high temperature microstructural stability of Ti-46Al-9Nb sheet material, Intermetallics. (2005). https://doi.org/10.1016/j.intermet.2004.09.001.

[14] A. Gorzel, G. Sauthoff, Diffusion creep of intermetallic TiAl alloys, Intermetallics. 7 (1999) 371–380. https://doi.org/https://doi.org/10.1016/S0966-9795(98)00099-5.

[15] W.T. Marketz, F.D. Fischer, H. Clemens, Deformation mechanisms in TiAl intermetallics - Experiments and modeling, Int. J. Plast. 19 (2003) 281–321. https://doi.org/10.1016/S0749-6419(01)00036-5.

[16] W. Harrison, Z. Abdallah, M. Whittaker, A model for creep and creep damage in the γ-titanium aluminide Ti-45Al-2Mn-2Nb, Materials (Basel). 7 (2014) 2194–2209. https://doi.org/10.3390/ma7032194.

[17] D. Peirce, R.J. Asaro, A. Needleman, Material rate dependence and localized deformation in crystalline solids, Acta Metall. 31 (1983) 1951–1976. https://doi.org/10.1016/0001-

6160(83)90014-7.
[18] R.J. Asaro, A. Needleman, Overview no. 42 Texture development and strain hardening in rate dependent polycrystals, Acta Metall. 33 (1985) 923–953. https://doi.org/10.1016/0001-6160(85)90188-9.
[19] P.E. McHugh, R. Mohrmann, Modelling of creep in a Ni base superalloy using a single crystal plasticity model, Comput. Mater. Sci. 9 (1997) 134–140. https://doi.org/10.1016/s0927-0256(97)00067-0.
[20] D.W. MacLachlan, L.W. Wright, S. Gunturi, D.M. Knowles, Constitutive modelling of anisotropic creep deformation in single crystal blade alloys SRR99 and CMSX-4, in: Int. J. Plast., 2001. https://doi.org/10.1016/S0749-6419(00)00058-9.
[21] I.N. Vladimirov, S. Reese, G. Eggeler, Constitutive modelling of the anisotropic creep behaviour of nickel-base single crystal superalloys, Int. J. Mech. Sci. (2009). https://doi.org/10.1016/j.ijmecsci.2009.02.004.
[22] L. Méric, P. Poubanne, G. Cailletaud, Single crystal modeling for structural calculations: Part 1-model presentation, J. Eng. Mater. Technol. Trans. ASME. (1991). https://doi.org/10.1115/1.2903374.
[23] A. Staroselsky, B.N. Cassenti, Combined rate-independent plasticity and creep model for single crystal, Mech. Mater. (2010). https://doi.org/10.1016/j.mechmat.2010.07.005.
[24] Y.S. Choi, T.A. Parthasarathy, C. Woodward, D.M. Dimiduk, M.D. Uchic, Constitutive model for anisotropic creep behaviors of single-crystal ni-base superalloys in the low-temperature, high-stress regime, Metall. Mater. Trans. A Phys. Metall. Mater. Sci. (2012). https://doi.org/10.1007/s11661-011-1047-7.
[25] V. Hasija, S. Ghosh, M.J. Mills, D.S. Joseph, Deformation and creep modeling in polycrystalline Ti-6Al alloys, Acta Mater. 51 (2003) 4533–4549. https://doi.org/10.1016/S1359-6454(03)00289-1.
[26] G. Venkatramani, S. Ghosh, M. Mills, A size-dependent crystal plasticity finite-element model for creep and load shedding in polycrystalline titanium alloys, Acta Mater. (2007). https://doi.org/10.1016/j.actamat.2007.03.017.
[27] H.Y. Kim, G. Wegmann, K. Maruyama, Effect of stress axis orientation on the creep deformation behavior of Ti-48Al polysynthetically twinned (PST) crystals, Mater. Sci. Eng. A. 329–331 (2002) 795–801. https://doi.org/10.1016/S0921-5093(01)01636-7.
[28] H.Y. Kim, K. Maruyama, Microstructure stability during creep deformation of hard-oriented polysynthetically twinned crystal of TiAl alloy, Metall. Mater. Trans. A Phys. Metall. Mater. Sci. 34 A (2003) 2191–2198. https://doi.org/10.1007/s11661-003-0282-y.
[29] G. Wegmann, K. Maruyama, On the microstructural stability of TiAl/Ti3Al polysynthetically twinned crystals under creep conditions, Philos. Mag. A Phys. Condens. Matter, Struct. Defects Mech. Prop. 80 (2000) 2283–2298. https://doi.org/10.1080/01418610008216473.
[30] H. Inui, K. Kishida, M. Misaki, M. Kobayashi, Y. Shirai, M. Yamaguchi, Temperature dependence of yield stress, tensile elongation and deformation structures in polysynthetically twinned crystals of Ti-Al, Philos. Mag. A Phys. Condens. Matter, Struct. Defects Mech. Prop. 72 (1995) 1609–1631. https://doi.org/10.1080/01418619508243933.
[31] K. Kishida, H. Inui, M. Yamaguchi, Deformation of lamellar structure in TiAl-Ti3Al two-phase alloys, Philos. Mag. A Phys. Condens. Matter, Struct. Defects Mech. Prop. 78 (1998) 1–28. https://doi.org/10.1080/014186198253660.
[32] Y. Umakoshi, T. Nakaimo, Plastic Behaviour of TiAl Crystals Containing a Single Set of Lamellae at High Temperatures, ISIJ Int. 32 (1992) 1339–1347. https://doi.org/10.2355/isijinternational.32.1339.
[33] K. Kishida, H. Inui, M. Yamaguchi, Deformation of PST crystals of a TiAl/Ti3Al two-phase

alloy at 1000°C, Intermetallics. 7 (1999) 1131–1139. https://doi.org/10.1016/S0966-9795(99)00033-3.
[34] J. Beddoes, W. Wallace, L. Zhao, Current understanding of creep behaviour of near ^{3}-titanium aluminides, Int. Mater. Rev. 40 (1995) 197–217. https://doi.org/10.1179/imr.1995.40.5.197.
[35] J. Pan, J.R. Rice, Rate sensitivity of plastic flow and implications for yield-surface vertices, Int. J. Solids Struct. 19 (1983) 973–987. https://doi.org/10.1016/0020-7683(83)90023-9.
[36] U.F. Kocks, Laws for work-hardening and low-temperature creep, J. Eng. Mater. Technol. Trans. ASME. 98 (1976) 76–85. https://doi.org/10.1115/1.3443340.
[37] H.J. Frost, M.F. Ashby, Deformation-mechanism maps, Pergamon Press, Oxford, Oxford, Pergamon Press. (1982). https://doi.org/10.1016/0378-3804(84)90015-9.
[38] A. Cornec, M.R. Kabir, N. Huber, Numerical prediction of the stress-strain response of a lamellar γTiAl polycrystal using a two-scale modelling approach, Mater. Sci. Eng. A. 620 (2015) 273–285. https://doi.org/10.1016/j.msea.2014.10.018.
[39] M. Werwer, A. Cornec, The role of superdislocations for modeling plastic deformation of lamellar TiAl, Int. J. Plast. 22 (2006) 1683–1698. https://doi.org/10.1016/j.ijplas.2006.02.005.
[40] M.F. Bartholomeusz, Q. Yang, J.A. Wert, Creep deformation of a two-phase TiAlTi3Al lamellar alloy and the individual TiAl and Ti3Al constituent phases, Scr. Metall. Mater. 29 (1993) 389–394. https://doi.org/https://doi.org/10.1016/0956-716X(93)90518-W.
[41] Y. Mishin, C. Herzig, Diffusion in the Ti-Al system, Acta Mater. 48 (2000) 589–623. https://doi.org/10.1016/S1359-6454(99)00400-0.
[42] F. Appel, R. Wagner, Interface-related deformation phenomena in intermetallic γ-titanium aluminides, Phys. Scr. T49B (1993) 387–392. https://doi.org/10.1088/0031-8949/1993/t49b/001.
[43] A.G. Evans, R.D. Rawlings, The Thermally Activated Deformation of Crystalline Materials, Phys. Status Solidi. 34 (1969) 9–31. https://doi.org/10.1002/pssb.19690340102.
[44] D.M. Dimiduk, P.M. Hazzledine, T.A. Parthasarathy, S. Seshagiri, M.G. Mendiratta, The role of grain size and selected microstructural parameters in strengthening fully lamellar TiAl alloys, Metall. Mater. Trans. A Phys. Metall. Mater. Sci. 29 (1998) 37–47. https://doi.org/10.1007/s11661-998-0157-3.
[45] B. Viguier, J. Bonneville, J.L. Martin, The mechanical properties of single phase γ Ti47Al51Mn2 polycrystals, Acta Mater. (1996). https://doi.org/10.1016/1359-6454(96)00073-0.
[46] F. Appel, R. Wagner, Microstructure and deformation of two-phase γ-titanium aluminides, Mater. Sci. Eng. R Reports. 22 (1998) 187–268. https://doi.org/10.1016/S0927-796X(97)00018-1.